frontiers | Frontiers in Mechanical Engineering

TYPE Original Research
PUBLISHED 12 January 2026
DOI 10.3389/fmech.2025.1739057

OPEN ACCESS

EDITED BY
Abdelmageed A. Elmustafa,
Old Dominion University, United States

REVIEWED BY
Hongjian Ni,
China University of Petroleum, China
Shaomin Li,
China Aerospace Science and Industry Corporation, China

*CORRESPONDENCE
Liu Huaiwei,
1294266503@qq.com
Zhu Zhigang,
1342793794@qq.com
Zhou Haina,
zhouhaina@gdcvi.net

RECEIVED 04 November 2025
REVISED 17 December 2025
ACCEPTED 22 December 2025
PUBLISHED 12 January 2026

CITATION
Qian L, Xuyong L, Huaiwei L, Zhigang Z, Hehong D, Guangjun L, Haina Z, Xuming F and Yuefei Z (2026) Structural design and vibration characteristics of a contra-rotating drilling tool based on planetary gear trains.
Front. Mech. Eng. 11:1739057.
doi: 10.3389/fmech.2025.1739057

Structural design and vibration characteristics of a contra-rotating drilling tool based on planetary gear trains

Li Qian[1], Liu Xuyong[2], Liu Huaiwei[3]*, Zhu Zhigang[3]*, Deng Hehong[2], Li Guangjun[4], Zhou Haina[3]*, Feng Xuming[5] and Zeng Yuefei[3]

[1]College of Environment and Civil Engineering, Chengdu University of Technology, Chengdu, China, [2]Guangdong Eagler Geological Equipment Technology Co., Ltd., Zhuhai, China, [3]Guangdong Construction Polytechnic, Guangzhou, China, [4]Guangdong Ruibo Architectural Design and Research Co., Ltd., Guangzhou, China, [5]Guangdong Zhenzheng Construction Engineering Testing Co., Ltd., Guangzhou, China

Introduction: To reduce severe drill string vibration and improve drilling efficiency in deep drilling, which are often accompanied by significant energy loss.
Method: The contra- rotation of the inner and outer drill bits was facilitated by planetary gear transmission, and the anti-torque fluctuation was reduced by the torque balance principle, thereby suppressing vibration. In this paper, the design of the gear, bearing, and seal structure of the contra-rotating drilling tool was completed; single rotation and contra-rotating drilling tools were prepared alongside artificial rock samples; a drilling test rig was constructed; and vibration signals of the drilling tools were collected at different rotation speeds.
Result: Time-domain and frequency-domain analyses revealed that the vibration acceleration amplitude of the contra-rotating drilling tool in the X, Y, and Z directions is significantly lower than that of the single rotation drilling tool. Furthermore, with increasing rotation speed, the vibration amplitude of the contra-rotating drilling tool remains stable or even decreases, whereas the vibration of the single rotation drilling tool increases significantly.
Discussion: A mechanistic analysis revealed that the contra-rotating drill bit requires less driving force to break rock, produces more shear failure zones, breaks rock more easily, and generates less vibration. This study provides an effective active control method for reducing drilling vibration and has good prospects for application in the field of engineering.

KEYWORDS

contra-rotating, drilling tool, structural design, vibration pattern, vibration reduction mechanism

1 Introduction

Deep geological exploration is extremely important for the national development of China. On the one hand, national development has increased the demand for deep mineral resource mining; on the other hand, deep exploration is also an essential promotional measure for earth science research. As the only technical method that can be used to obtain deep geological objects, drilling is currently among the most difficult exploration

techniques. During the drilling process, the drill string, as a key component that transmits driving force to the drill bit, is simultaneously subjected to axial pressure, torque, and bending moment, thus making the corresponding forces and motions very complex. In addition, the friction between the drill string and the well wall can easily cause vibration of the drill string.

Drill string vibration can be divided into three basic forms: vertical, lateral, and torsional vibrations. Furthermore, these three vibrations always exist downhole and influence each other. Severe drill string vibration causes fatigue failure of the drilling tool, which creates complicated drilling conditions, significantly prolonging construction time and increasing construction cost. Moreover, drill string vibration consumes a large amount of energy that should have been used to cut rocks, thereby causing a large amount of energy waste. Therefore, unfavorable drill string vibration greatly increases the cost of conventional drilling while reducing the drilling efficiency; thus, effective vibration reduction is highly important for reducing the cost of drilling.

In accordance with vibration reduction theory, vibration control methods can be divided into passive control and active control (Dong and Chen, 2016). Early methods of passive vibration reduction in drill strings were achieved by reducing drill pipe resonance. Bailey and Remmert (2010) improved a new type of BHA by removing the near-bit stabilizer and moving the roller reamer from the drill collar to the heavy-weight drill pipe. This effectively controls drill string resonance and stick-slip. Installing shock absorbers is another major way to passively control the drill string system. Gao & Huang. (2024) pointed out that installing a vibration damping tool on the drill string generates a periodic excitation force, which can significantly reduce the frictional resistance of the pipe string movement and alleviate the frequent sticking and jamming problems during drilling. Lv (2020) designed a tubular downhole logging tool vibration damper that can effectively suppress the lateral vibration of the drill string system and reduce the influence of rotational speed on vibration. Hu et al. (2022) studied the vibration damping effect of the damper on the upper drill string and the lower drill bit, using the dynamic process of rock breaking by the drill bit as the bottom hole boundary condition. In addition to the two passive control methods mentioned above, changing the energy distribution is also an effective way to passively control drill string vibration.

Active control of drill string vibration refers to the process of applying energy to the exterior of the drill string during vibration, based on detected vibration signals. Using a specific control strategy and real-time calculations, a controller is driven to suppress or eliminate the vibration. By optimizing the gain coefficients of a proportional-derivative (PD) controller, Ritto and Ghandchi-tehrani (2019) obtained a stability region diagram for torsional motion when both drilling pressure and top drive speed change simultaneously. Based on the coupled longitudinal and torsional vibrations of the drill string, Zhang (2020) considered the time-delay effect in the dynamic model and designed a PD feedback controller for torsional vibration and a state observer to estimate the axial motion, achieving good control results. Tashakori et al. (2022) proposed a time-delay feedback control method with a state observer and predictor, using the traveling block speed and top drive torque as control inputs to control the longitudinal and torsional motion of the drill string. Jia (2021) building upon LQR modal control, incorporated piezoelectric control. Through simulations of the drill string system dynamics, the results showed that LQR control can effectively suppress drill pipe whirling. Based on adaptive control principles, Huang et al. (2019) and Zhou (2021) respectively designed a model-reference adaptive controller and an adaptive feedforward active vibration control system for drill pipes, and experimentally verified the vibration reduction effect of the designed active control systems. Based on fuzzy theory, Abdelbasset et al. (2022) proposed a robust active controller based on fuzzy sliding mode control (FSMC), and the test results revealed that this controller was superior to the traditional controller in terms of dynamic performance and stable error. Based on robust control theory, Cai et al. (2022) designed a trajectory control system based on equivalent input disturbance, using two control loops to track and control the inclination and azimuth of the trajectory, respectively. Ma et al. (2023) proposed a robust integrated control design to suppress fluctuations in drilling pressure. Noabahar Sadeghi and Arikan (2022) proposed that adjusting the drilling pressure and increasing the damping at the bottom of the drill string have a better control effect on stick-slip motion. Maclean et al. (2022) proposed an improved integral resonant controller with a tracker, which can effectively suppress stick-slip motion and has good robustness. Lu et al. (2023), based on a multi-degree-of-freedom lumped parameter model, designed a dynamic output feedback method that only utilizes ground measurement data and considers the time delay induced by regenerative cutting and actuator saturation to control the longitudinal-torsional coupled vibration of the drill string.

In addition to traditional areas, Intelligent control technology is currently in a stage of rapid development and has broad application prospects. Although research applying neural networks and artificial intelligence technology to drill string vibration control is still in its early stages, it has become a new research direction in the field of drill string vibration control. Wang et al. (2024) pointed out that with the continuous advancement of data acquisition and processing technologies and the integration of multi-source data from surface and downhole, machine learning can significantly improve the accuracy and reliability of drill string vibration identification and prediction. Hegde et al. (2019) proposed an optimization algorithm that combines ROP optimization with a machine learning-based vibration model, incorporating various extreme vibration modes as constraints to ensure that the optimized drilling parameters not only improve ROP but also prevent excessive vibration. Feng (2019) designed a top drive controller to control the vibration of the drill string system and developed a genetic algorithm to optimize the position of the bottom hole assembly stabilizer, aiming to suppress drill string vibration.

With respect to the two vibration reduction methods, active vibration reduction is used mainly to reduce the generation of vibration by controlling the vibration source, whereas passive vibration reduction is mainly used to reduce the vibration amplitude with a certain structure or process after vibration is generated. In principle, active vibration reduction can produce a more obvious vibration reduction effect. Current active vibration reduction technologies are primarily aimed at optimizing the design of bit and cutter structures, and relatively few drilling tools can achieve active vibration reduction. Based on an investigation of vibration reduction technology during the rotation process, contra-rotating technology has a broad range of applications in eliminating anti-torque in helicopters and propeller-driven vehicles, such as

10.3389/fmech.2025.1739057

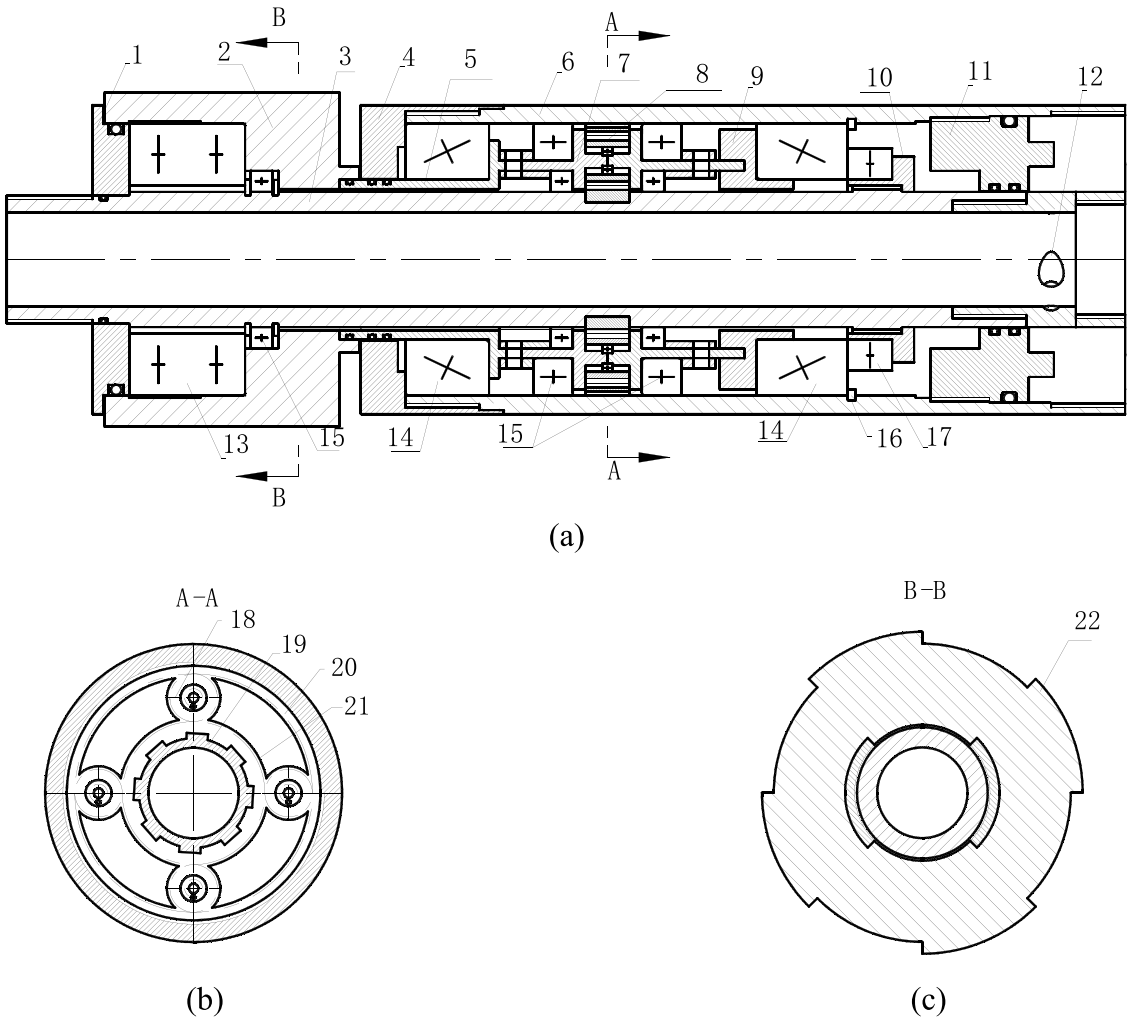

FIGURE 1
(a): overall structural design for entire tool; **(b)**: cross-sectional structure for section A-A; **(c)**: cross-sectional structure for section B-B.

underwater torque-balanced propellers and coaxial dual-rotor helicopters. Therefore, as reported in this paper, a contra-rotating drilling tool based on a planetary gear train was developed. Based on the principle of torque balance, the contra-rotating drilling tool uses two drill bits on the same axis, with the inner and outer bits rotating in opposite directions. Contra-rotating drilling can reduce the reaction force of the bit and torque fluctuations generated by the friction between the drill bit and the stratum, thereby reducing vibration. In addition to the mechanism design, corresponding test equipment was used to measure and analyze the vibration patterns of both the contra-rotating and single rotation drilling tools.

2 Design of the contra-rotating drilling structure

2.1 Overall structural design

The overall structure of the contra-rotating drilling tool is illustrated in Figure 1. The contra-rotation of the inner and outer drill bits is facilitated mainly by a planetary gear train, and the structure consists mainly of a double-layer drill pipe structure (the inner and outer drill pipes are fixed by a ring gear), the planetary gear train, the bearings between the inner and outer drill pipes, and seals. In the working state, the power motor drives the inner drill pipe, which is fixed to the gear to rotate clockwise; the planetary gear carrier is constrained from rotating by the fixed housing (2); and the planetary gear drives the outer drill pipe, which is fixed to the outer ring gear to rotate counterclockwise. In light of the requirement of confidentiality, only the structure is described, whereas the specific parameters are not described in detail.

The core of the contra-rotating drilling tool is the planetary gear train shown in Figure 1b, which consists of a sun gear (21), planetary gears (18), and an outer ring gear (20). The sun gear (21) and outer ring gear (20) are fixed to the inner drill pipe and the outer drill pipe, respectively, by splines. The planetary gears (18) are mounted on the gear carrier (7), and the gear carrier (7) is fixed to the fixed housing (2) through the fixed housing connector (5). The shape of the fixed housing (2) is shown in Figure 1c, and the maximum dimension is slightly larger than the outer diameter of the outer drill pipe (6).

During the drilling process, the fixed housing (2) can be kept motionless as a result of the frictional resistance between it and the well wall, such that the planetary gear carrier (7) remains motionless, and the planetary gears only rotate but do not revolve when the planetary gears mesh with the sun gear. When power is input from the inner drill pipe (3), to which the sun gear (21) is fixed, the sun gear (21) drives the planetary gear (18) to rotate. The planetary gear (18) is constrained by the gear carrier (7) to only rotate, which causes the outer drill pipe (6), fixed to the outer gear ring (20), to rotate in the opposite direction to that of the inner drill pipe (3), thereby achieving contra-rotation.

Bearings are used between the inner and outer drill pipes to support the relatively separated drill pipes. Radial contact bearings are used inside the fixed housing and the upper and lower ends of the planetary carrier to support them, a tapered roller bearing with a retaining ring is used at the lower end of the planetary carrier to support the axial thrust from the outer drill pipe, and a thrust bearing is used inside the fixed housing and the seal (1) at the upper end to restrict the motion of the drill pipe. Rotation occurs between the inner and outer drill pipes of the contra-rotating drilling tool, and an O-ring is used to seal the gap between them. A nozzle is provided at the connection between the inner drill pipe and the inner bit to ensure that the drilling fluid can fully flow into the gap between the inner and outer bits.

2.2 Design of the gear structure

The transmission component of the contra-rotating drilling tool is driven by a planetary gear train, and the transmission route is as follows: driving motor–contra-rotating inner drill pipe–planetary gear train–contra-rotating outer drill pipe. The planetary gear train consists of a sun gear, planetary gears, an outer ring gear, and a planetary carrier. The number of planetary gears depends on the design load, typically ranging from three to four; in this study, four such gears are used.

The number of planetary gears is not arbitrarily chosen, but rather based on a comprehensive consideration of the expected working load of the drill string and downhole space constraints, primarily according to the following:

First, based on load distribution and transmission smoothness. Under given drilling pressure and torque load conditions, using four planetary gears distributes the load across more meshing points. Compared to the common three-gear scheme, this effectively reduces the contact stress and bending stress of individual gears and their supporting bearings, improving the overall system load-bearing capacity and fatigue life. Simultaneously, the even-numbered and symmetrical layout helps improve the dynamic balance of the system, suppressing periodic vibrations that may be induced by uneven load distribution in the transmission links.

Second, balancing structural compactness and downhole space constraints. The planetary gear system must be accommodated within the limited annular space between the outer and inner tubes of the drill string. The four-gear scheme achieves good load distribution while requiring a more compact outer gear diameter and radial space compared to schemes with five or more gears. This ensures that the overall outer diameter of the tool meets conventional wellbore size constraints and provides sufficient space for the arrangement of critical components such as bearings and seals.

Finally, focusing on system reliability and force flow symmetry. For the complex variable load conditions in deep well drilling, four planetary gears form a statically determinate and highly symmetrical force transmission system. This layout has excellent self-adaptability, achieving good load sharing even with minor manufacturing and assembly errors, avoiding single-point overload, and thus significantly improving the operational reliability of the transmission chain under harsh conditions.

In summary, the selection of four planetary gears represents the optimal balance between load-bearing capacity, space constraints, and operational reliability. The planetary gears are evenly distributed within the gear train. Because the inner and outer drill bits need to rotate in opposite directions, the planet carrier is designed to be fixed (non-rotating). Therefore, the planetary gears only rotate on their own axes during transmission and do not revolve around the central axis. The gear type used in this design is involute spur gear.

Each planetary gear is evenly distributed in the gear train. Since the inner and outer bits need to rotate in opposite directions, the planetary carrier cannot rotate, and the planetary gears do not revolve but rather only rotate. The gear type used in this design is an involute cylindrical gear. The planetary gear train inside the contra-rotating drilling tool is placed horizontally. Compared with a vertical placement, the load distribution of the horizontal gear train is more uniform. Therefore, in the calculation, the circumferential forces transmitted between the four planetary gears and the sun gear/outer ring gear are distributed equally; that is, each planetary gear experiences an equal circumferential force, and the sum of the circumferential forces acting on all four planetary gears equals the circumferential force acting on the sun gear and outer ring gear.

2.3 Bearing structure design

In the contra-rotating drilling tool structure, the inner and outer drill pipes are separated; thus, bearings are needed to support the structure. The bearings used in the structure are shown in Figure 2. Radial contact bearings (7 and 8) are used between the inner drill pipe and planetary carrier (10) and between the outer drill pipe and planetary carrier (10) to support the planetary carrier and the inner and outer drill pipes, respectively. A radial contact bearing (4) is similarly installed between the fixed housing and the inner drill pipe to support them. This radial contact bearing is a deep groove ball bearing that mainly bears radial load. Owing to the relative rotational motion of the inner and outer drill pipes of the contra-rotating drilling tool, it is necessary to provide bearings that can withstand the axial force to limit the axial relative motion between the inner and outer drill pipes. Therefore, a tapered roller bearing (12) is positioned at the lower ends of the inner and outer drill pipes, and the bearing is locked by a retaining ring. A thrust ball bearing (2) is also positioned at the fixed housing to withstand the axial pressure from the outer drill pipe, and the bearing is blocked by a retaining cover (1) that is fixed to the inner drill pipe. The rotation of the gear is supported by a radial contact bearing (9) between the gear and the planetary carrier.

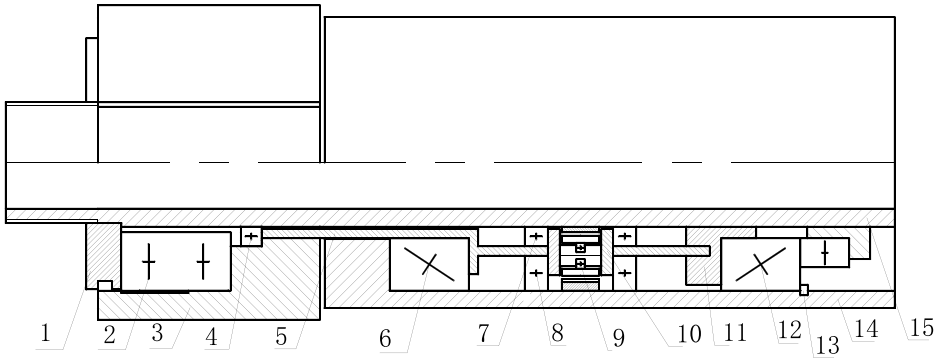

FIGURE 2
Bearing design diagram. (1—retaining cover; 2—thrust bearing; 3—fixed housing; 4—radial contact bearing a; 5—fixed housing connector; 6—tapered roller bearing a; 7, 8, and 9—radial contact bearings b, c, and d; 10—planetary carrier; 11—bearing housing; 12—tapered roller bearing; 13— retaining ring; 14—outer drill pipe; 15—inner drill pipe).

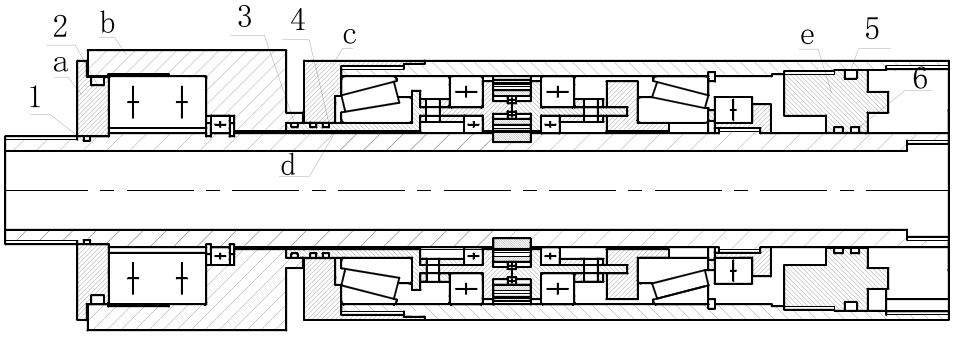

FIGURE 3
Schematic diagram of the sealing of the contra-rotating drilling tool. (1, 3, and 5—static seals; 2, 4, and 6—rotary dynamic seals; a—stationary housing seal; b—fixed housing; c—rotary housing seal; d—fixed housing connector; e—lower seal).

2.4 Design of the sealing structure

Based on the rotary sealing requirements designed in this paper, the three most common sealing methods are O-ring sealing, mechanical sealing, and oil sealing. Mechanical seals and oil seals are both excellent for rotary seals, but the sealing pressure of oil seals is low (standard oil seals are rated for pressures below 0.05 MPa, while pressure-resistant oil seals are rated for 1–1.2 MPa). The sealing pressure of conventional drilling is related to the depth. At 260 m, the ambient pressure exceeds 3 MPa; moreover, conventional drilling beyond 1000 m has become standard practice. Therefore, it is difficult for the oil seal to meet the demand for drilling. Mechanical seals can be used in high-pressure environments, but their structures are complicated, and they are both large in volume and expensive. The downhole space is limited; thus, mechanical seals with complex structures and large volumes are not suitable. O-rings are small, simple in structure, low in cost, widely used, convenient to disassemble and assemble, and easy to replace; therefore, the O-ring was chosen as the seal for the contra-rotating drilling tool.

The sealing design of the contra-rotating drilling tool is shown in Figure 3. Seal a of the fixed housing and the inner drill pipe rotate synchronously, and fixed housing b does not rotate. Therefore, an O-ring is used as the static seal between seal a of the fixed housing and the inner drill pipe, and an O-ring is used as a rotating dynamic seal between the seal and the fixed housing. Seal c of the rotary housing rotates synchronously with the outer drill pipe, and fixed housing connector d does not rotate. Therefore, an O-ring is used as a static seal between fixed housing b and fixed housing connector d, and an O-ring is used as a rotary dynamic seal between fixed housing connector b and rotary housing seal c. Seal e is set at the bottom of the contra-rotating drilling tool to seal the gap between the inner and outer drill pipes, and the seal rotates synchronously with the outer drill pipe. Finally, an O-ring is used as a static seal between the seal and the outer drill pipe, and an O-ring is used as a rotary dynamic seal between the inner drill pipe and the seal.

3 Design and fabrication of the experimental setup

3.1 Test purpose

To investigate the vibration patterns of the contra-rotating drilling tool designed in this paper during drilling, the tool was

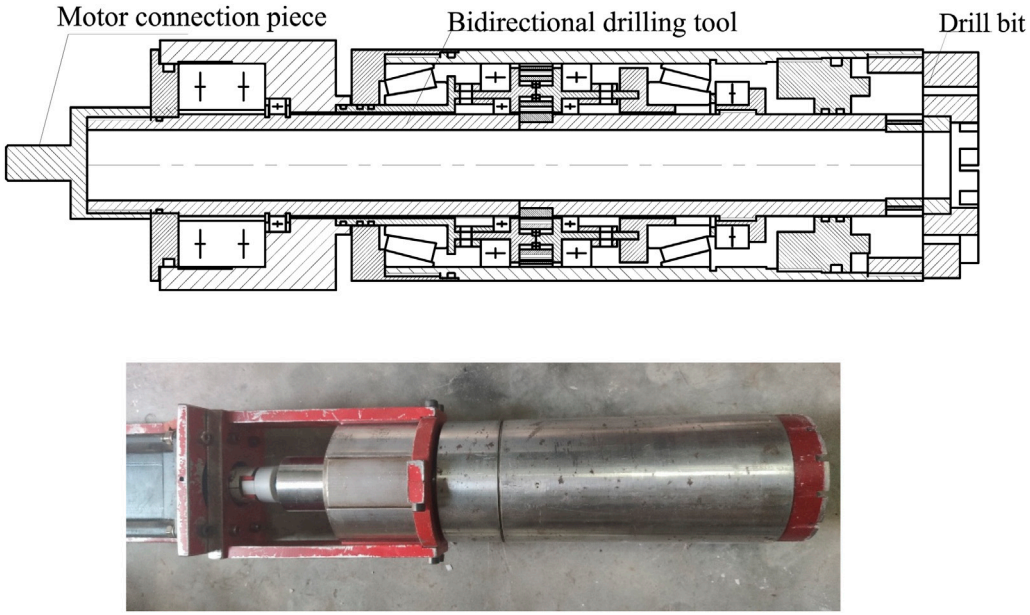

FIGURE 4
Overall assembly diagram (upper) and fabricated piece (lower) of the contra-rotating drilling tool.

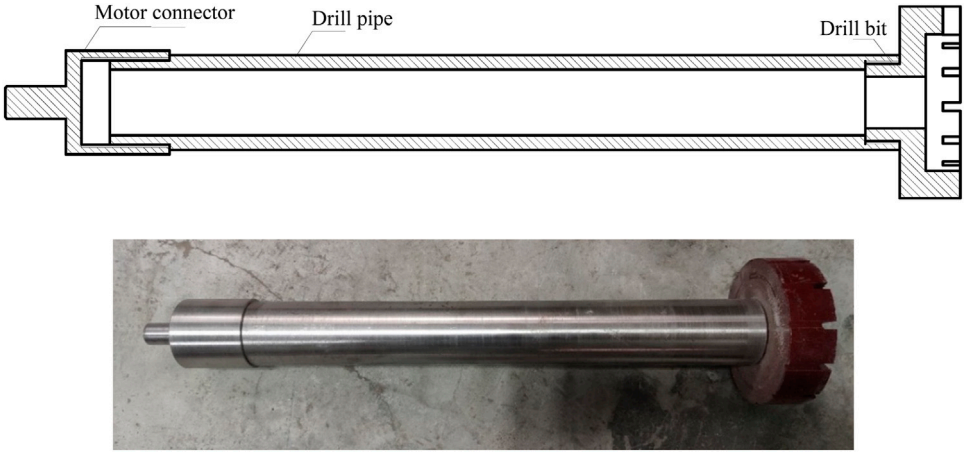

FIGURE 5
Overall assembly diagram (upper) and fabricated piece (lower) of the single rotation drilling tool.

manufactured according to drawings, and a corresponding conventional single rotation drilling tool was fabricated for the purpose of comparison. Drilling tests were conducted using both tools on the designed drilling test rig. Vibration acceleration during drilling was measured using vibration sensors. An analysis of time-domain and frequency-domain results revealed differences in vibration patterns between the two tools during drilling.

3.2 Fabrication of single rotation and contra-rotating drilling tools

Based on the structural design of the contra-rotating drilling tool, the parts in the structure were fabricated according to drawings; furthermore, a single rotation rotary drilling tool was fabricated. The single rotation rotary drilling tool includes only the drill pipe and the drill bit at the lower end. A schematic diagram and fabricated piece of the contra-rotating drilling tool are shown in Figure 4, and a schematic diagram and fabricated piece of the single rotation drilling tool are shown in Figure 5.

3.3 Machining of the single rotation and contra-rotating bits

According to the size of the actual diamond bit, the inner and outer diameters of the inner and outer bits are 49 mm and 77 mm and 79 mm and 122 mm for the contra-rotating drill,

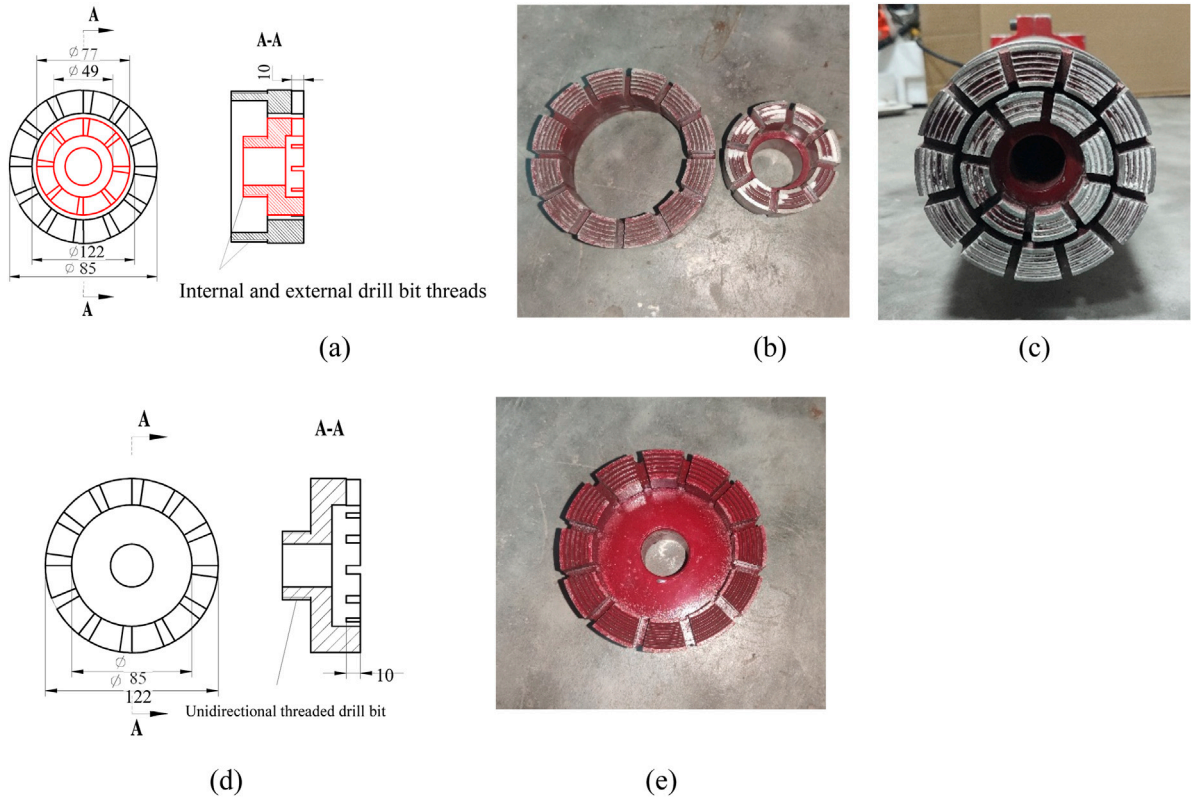

FIGURE 6
2D drawings and fabricated pieces of single rotation and contra-rotating drill bits. ((**a**) 2D drawing of the contra-rotating drill; (**b,c**) schematic diagram of the fabrication and installation of the contra-rotating drill; (**d**) 2D drawing of the single rotation drill; (**e**) the fabricated single rotation drill).

respectively. The inner bit has 8 teeth, and the outer bit has 12 teeth. The size of the bit of the single rotation drill is the same as that of the outer bit of the contra-rotating drill, with inner and outer diameters of 79 mm and 122 mm, respectively, and the single rotation drill bit has 12 teeth. Figure 6 presents the two-dimensional (2D) drawings and fabricated pieces of the single rotation and contra-rotating drill bits.

3.4 Rock sample processing and preparation

Artificial rock samples were used in the drilling test because they exhibit better homogeneity and adjustable strength. The composition of the rock sample is as follows: quartz accounts for 40% of the total content, clay and cement together account for 40% of the total content, with a clay to cement ratio of 2:1, and calcite and dolomite jointly account for 20% of the total content, with a calcite to dolomite ratio of 13:8. The rock samples were cured in a standard curing room, with a room temperature of 20 °C ± 2 °C and humidity of >95%. The size and physical and mechanical properties of the artificial rock samples are as follows: Since the nominal diameters of the outer bits of both the contra-rotating drill and the single rotation drill are 122 mm, the rock samples were designed with a length and width approximately three times the diameter of the drill bit to minimize boundary effects. The artificial rock sample is a cuboid with a length, width, and height of 360 × 360 × 150 mm. The processed artificial rock sample is shown in Figure 7, and the physical and mechanical properties are presented in Table 1.

FIGURE 7
Schematic diagram of the artificial rock sample.

The specific mix ratio and mechanical parameters were chosen to create a homogeneous, fractured standard experimental medium to focus on comparing the performance differences of two drill bit structures under identical, controlled formation conditions. Further research will require the use of a series of rock samples with varying

10.3389/fmech.2025.1739057

TABLE 1 Physical and mechanical properties of the artificial rock sample.

Material	Density/kg/m^3	Elastic modulus/GPa	Poisson's ratio	Internal friction angle/°	Tensile strength/MPa
Artificial rock sample	2278	2.684	0.224	39.1	2

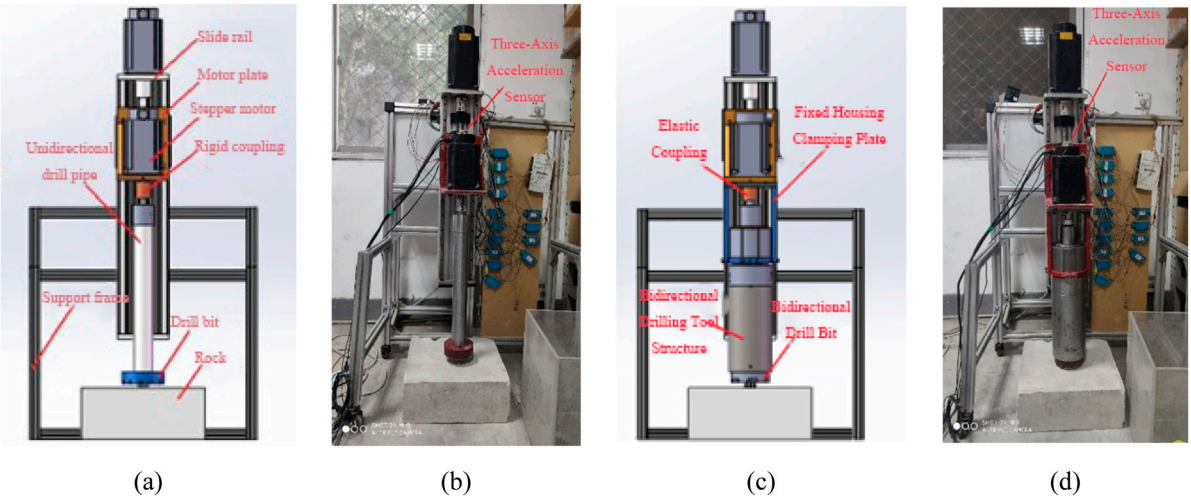

FIGURE 8
Schematic diagrams of the model and physical drilling test rig. ((**a**) Schematic diagram of the single rotation drilling tool test rig; (**b**) the physical single rotation drilling tool test rig; (**c**) schematic diagram of the contra-rotating drilling tool test rig; (**d**) the physical contra-rotating drilling tool test rig).

strengths and abrasive properties to explore the boundary effects of lithological variations on the vibration reduction effect of the counter-rotating drill bit.

3.5 Construction of the test rig

The drilling test rig used in this paper consists mainly of a sliding guide rail and a bracket that can move up and down, as shown in Figure 8. The slider on the sliding guide rail can move up and down through the spiral guide rail and the stepper motor. The sliding guide rail is supported and fixed by a bracket, and the motor that drives the drilling tool to rotate is connected with the slider through a motor board. Single rotation and contra-rotating drilling tools are mounted on the slider through the motor board, and the up and down motions of the single rotation and contra-rotating drilling tools are controlled by the sliding guide rail. The drilling tool is connected to the stepper motor through a connecting piece, and the rotation speed of the drilling tool is controlled by the stepper motor. Because the contra-rotating drilling tool is heavy and the coupling cannot support the vertical load, a clamping plate was included between the fixed housing and the motor mounting plate and designed to support the weight of the drilling tool at its lower end. And the entire frame has been connected to the wall behind it to increase stability.

The drill pipe and the drill bit at the lower end rotate during the drilling test, and the triaxial acceleration sensor relies on a cable to transmit data; therefore, the sensor cannot be directly mounted on the drilling tool structure or drill bit. Considering the direct contact between the motor that provides torque to the drill tool and the drill tool itself, the triaxial accelerometer was mounted on the upper surface of the stepper motor, as shown in Figure 8b,d.

It should be noted that the vibration acceleration amplitude measured in this experiment reflects not only the interaction between the drill bit and the rock, but also the dynamic response of the test rig system itself. However, since the unidirectional and bidirectional rotating drill bits were tested under completely identical test platform and rock sample conditions, the comparison of the vibration signals between the two effectively reveals the inherent differences in vibration suppression capabilities of the different structures.

4 Time-domain comparison of single rotation and contra-rotating drilling tool vibration signals

4.1 Time-domain comparison of vibration at a rotation speed of 30 r/min

The vibration triaxial acceleration of the two drilling tools at 30 r/min was determined using a triaxial acceleration sensor, as shown in Figure 9. A comparison of the three directions reveals that the vibration acceleration of the two drilling tools clearly exhibits a distinct pattern of $X \approx Y > Z$. The main cause of this characteristic lies in the installation position of the vibration sensor. The vibration in the X and Y directions reflects the vibration in the horizontal

10.3389/fmech.2025.1739057

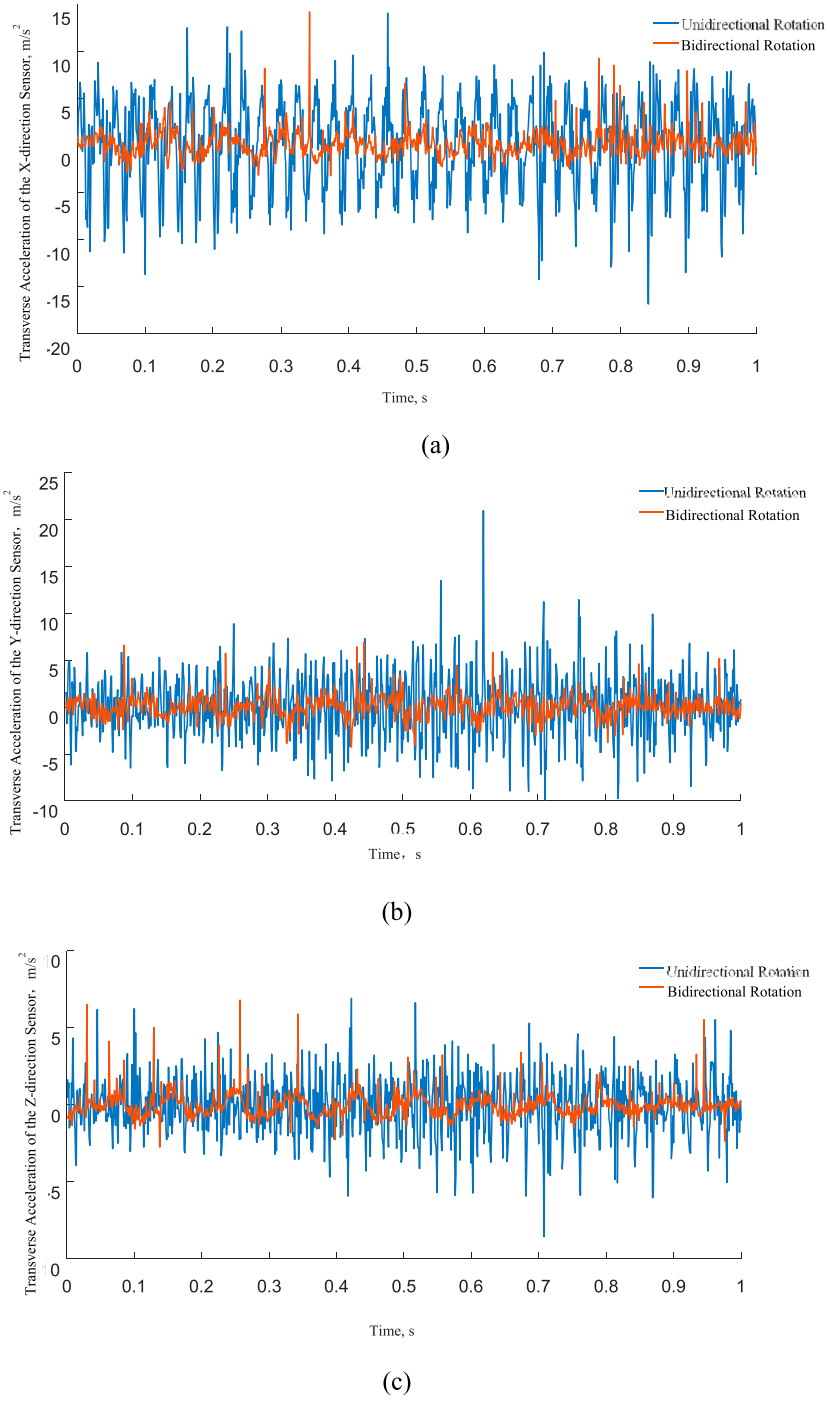

FIGURE 9
Comparison of the acceleration of the single rotation and contra-rotating drilling tools at a rotation speed of 30 r/min. (**(a)** acceleration in the X direction; **(b)** acceleration in the Y direction; **(c)** acceleration in the Z direction).

direction, and the vibration in the Z direction reflects the vibration in the vertical direction. In this test, since the power machine is controlled by the sliding rail, the sliding rail is fixed on the main frame, thus enabling it to offset part of the vibration in the Z direction to a certain extent.

A comparison of the vibration acceleration ranges of the two drilling tools reveals that, following the removal of occasional discrete fluctuations, the vibration acceleration of the contra-rotating drilling tool in the X/Y/Z directions is significantly lower than that of the single rotation drilling tool. In the *X* direction, the vibration acceleration of the single rotation drilling tool is concentrated mainly in the range of −3.8–2.8 m/s^2, the acceleration of the contra-rotating drilling tool is in the range of −0.72–0.76 m/s^2, and the vibration acceleration range of the

10.3389/fmech.2025.1739057

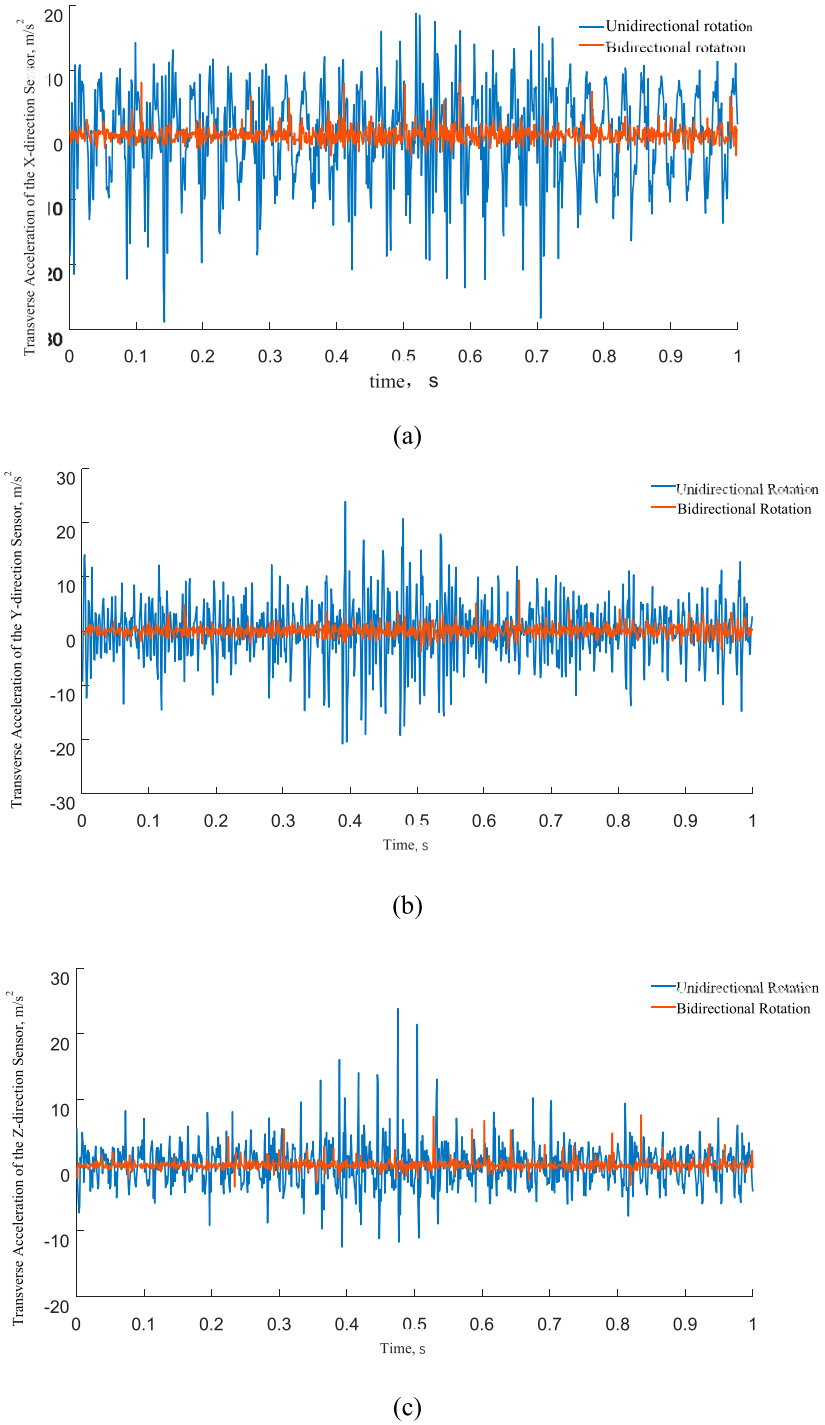

FIGURE 10
Comparison of the acceleration of the single rotation and contra-rotating drilling tools at a rotation speed of 60 r/min. ((**a**) acceleration in the X direction; (**b**) acceleration in the Y direction; (**c**) acceleration in the Z direction).

contra-rotating drilling tool in the *X* direction is only 22% that of the single rotation drilling tool. In the *Y* direction, the vibration acceleration of the single rotation drilling tool is concentrated mainly in the range of −1.8–2.2 m/s^2, the acceleration of the contra-rotating drilling tool is concentrated in the range of −0.53–0.69 m/s^2, and the vibration acceleration range of the contra-rotating drilling tool in the *Y* direction is only 31% that of the single rotation drilling tool. In the *Z* direction, the vibration acceleration of the single rotation drilling tool is concentrated mainly in the range of -1–1.1 m/s^2, the acceleration of the contra-rotating drilling tool is concentrated in the range of −0.53–0.27 m/s^2, and the vibration acceleration range of the contra-rotating drilling tool in the *Z* direction is only 38% that of the single rotation drilling tool.

4.2 Time-domain comparison of vibration at a rotation speed of 60 r/min

The acceleration signals measured for the single rotation and contra-rotating drilling tools at 60 r/min are shown in Figure 10. The vibration patterns in the three directions are very similar to those observed under the condition of 30 r/min, and the vibration acceleration of the two drilling tools clearly exhibits a distinct pattern of X ~ Y > Z. The comparison of the two drilling tools shows that the vibration amplitude of the contra-rotating drilling tool is also significantly lower than that of the single rotation drilling tool at 60 r/min. In the *X* direction, the vibration of the contra-rotating drilling tool is stable in the range of −0.7–0.6 m/s^2, the vibration of the single rotation drilling tool is concentrated in the range of −3.9–5.3 m/s^2, and the vibration acceleration range of the contra-rotating drilling tool in the *X* direction is only 14% that of the single rotation drilling tool. In the *Y* direction, the vibration acceleration of the single rotation drilling tool is concentrated mainly in the range of −2.7–3 m/s^2, the vibration acceleration of the contra-rotating drilling tool is in the range of −0.5–0.6 m/s^2, and the vibration acceleration range of the contra-rotating drilling tool in the *Y* direction is only 19% that of the single rotation drilling tool. In the *Z* direction, the vibration acceleration of the single rotation drilling tool is concentrated mainly in the range of −2.1–1.6 m/s^2, the vibration acceleration of the contra-rotating drilling tool is concentrated mainly in the range of −0.3–0.2 m/s^2, and the vibration acceleration range of the contra-rotating drilling tool in the Z direction is only 14% that of the single rotation drilling tool.

A comparison of the vibration acceleration ranges of the contra-rotating drilling tool and single rotation drilling tool under the two rotation speeds revealed that when the rotation speed was changed from 30 r/min to 60 r/min, the vibration amplitude of the contra-rotating drilling tool essentially did not increase and remained at a similar level ([-0.5, 0.6] m/s^2 interval in the *X*/*Y* directions and [-0.5, 0.2] m/s^2 interval in the *Z* direction). However, the vibration associated with the single rotation drilling tool exhibited significant intensification. The acceleration amplitude range in the *X* direction increased by 30%, the acceleration amplitude range in the *Y* direction increased by 30%, and the acceleration amplitude range in the *Z* direction increased by 55%, indicating that the vibration acceleration of the single rotation drilling tool clearly increased with increasing speed. Assuming that the vibration acceleration of the contra-rotating drilling tool remains essentially unchanged, it can thus be inferred that as the rotation speed increases, the tool's effect on vibration control becomes increasingly pronounced.

5 Frequency-domain comparison of the vibration signals of the single rotation and contra-rotating drilling tools

5.1 Frequency-domain vibration signal at 30 r/min

A Fast Fourier transform (FFT) was performed on the vibration acceleration signals of the single rotation and contra-rotating drilling tools obtained in the test. The acceleration signal measured at a rotation speed of 30 r/min was subjected to FFT to obtain the frequency domain signal, as shown in Figure 11. The peak value in the figure represents the frequency contained in the signal. During drilling, the main frequency of the contra-rotating drilling tool is 11 Hz. The acceleration amplitudes of the main signals in the *X*/*Y*/*Z* directions are relatively similar, measuring 0.61, 0.63, and 0.51 m/s^2, respectively. Furthermore, during drilling, the main frequencies of the single rotation drilling tool are 38 Hz and 112 Hz. The main frequency obtained by the FFT of the acceleration signal of the single rotation drilling tool is higher than that of the contra-rotating drilling tool. The vibration of the single rotation drilling tool is more intense during drilling; therefore, the frequency of the collected acceleration is relatively high. At 38 Hz, the acceleration amplitudes in the *X*/*Y*/*Z* directions are 3.78, 0.53, and 0.55 m/s^2, respectively, and at 112 Hz, the acceleration amplitudes in the X/*Y*/*Z* directions are 0.5, 1.4, and 0.84 m/s^2, respectively. The results reveal that at 30 r/min, the main frequency of the contra-rotating drilling tool is lower than that of the single rotation drilling tool; in addition, the amplitude is smaller than that of the single rotation drilling tool.

5.2 Frequency-domain analysis of vibration at 60 r/min

An FFT was performed on the measured acceleration signal at a rotation speed of 60 r/min to obtain the frequency domain signal, as shown Figure 12. During drilling, the main frequency of the contra-rotating drilling tool is 300 Hz, and the acceleration amplitudes in the *X*/*Y*/*Z* directions are 0.49, 0.44, and 0.22 m/s^2, respectively. The main frequencies of the single rotation drilling tool at 60 r/min are 37 Hz and 109 Hz. At 36 Hz, the frequency acceleration amplitudes in the X/Y/Z directions are 7 m/s^2, 0.56 m/s^2, and 1.23 m/s^2, respectively, and at 109 Hz, the acceleration amplitudes in the X/Y/Z directions are 0.14 m/s^2, 2.99 m/s^2, and 1.55 m/s^2, respectively. At 60 r/min, the main frequency of the contra-rotating drilling tool is greater than that of the single rotation drilling tool, and its amplitude is much lower than that of the single rotation drilling tool.

A comparison of the results at 30 r/min and 60 r/min showed that the dominant frequency of single rotation drilling tool vibration remains essentially unchanged, and the only difference is that the maximum amplitude of the corresponding dominant frequency increases by 85.1%, 113.6%, and 123.6% in the X/Y/Z directions, respectively. For the contra-rotating drilling tool, at 60 r/min, the dominant frequency significantly shifts backward compared with that at 30 r/min, from 11 Hz to 300 Hz. Moreover, the amplitude of the dominant frequency of the vibration of the contra-rotating drilling tool decreases significantly, with the change rates in the X/Y/Z directions being −19.7%, −30.1%, and −56.7%, respectively. The comparison reveals that as the rotation speed increases, the vibration of the single rotation drilling tool increases significantly, whereas the vibration of the contra-rotating drilling tool decreases significantly. Therefore, the contra-rotating drilling tool undoubtedly offers greater advantages in terms of vibration reduction under high rotation speeds.

10.3389/fmech.2025.1739057

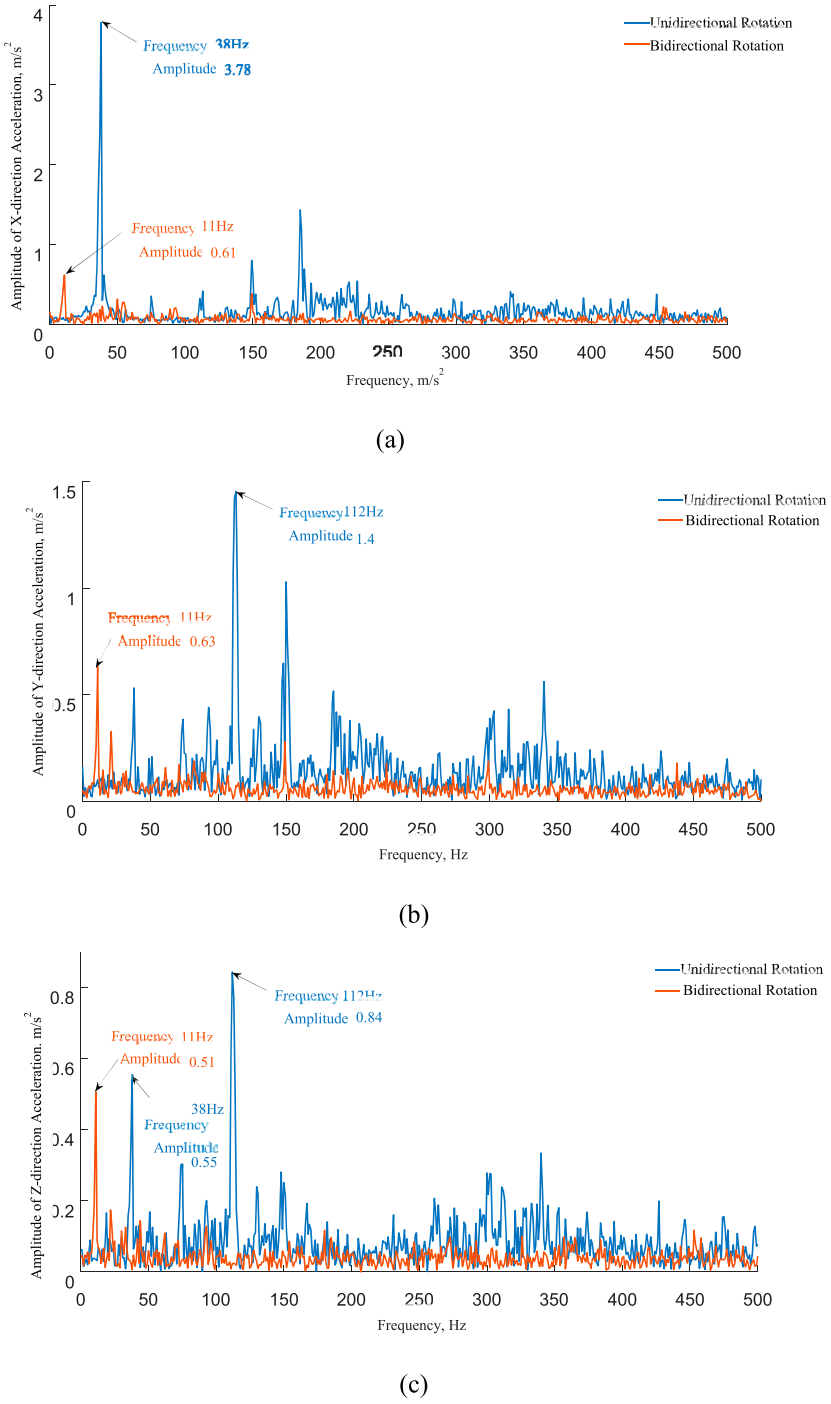

FIGURE 11
Frequency amplitude curve of the single rotation and contra-rotating drilling tools at 30 r/min. (**(a)** X direction; **(b)** Y direction; **(c)** Z direction).

6 Vibration reduction mechanism of the contra-rotating drilling tool

According to the time domain and frequency domain analysis results, compared with the contra-rotating drilling tool, the single rotation rotary drilling tool results in significantly more vibration, and this vibration exhibits an increasing trend as rotational speed increases. This pattern is the result of the different cutting processes of the two drilling tools on the stratum.

To analyze the interaction between the drill bit and the rock unit, a simplified model is used as shown in Figure 13. The localized rock fracture occurring beneath a single cutting tooth of the drill bit is considered as an independent rock unit. Before fracturing, this rock unit is constrained from below and laterally by the surrounding rock mass. To simplify the analysis, it is assumed that the resultant

10.3389/fmech.2025.1739057

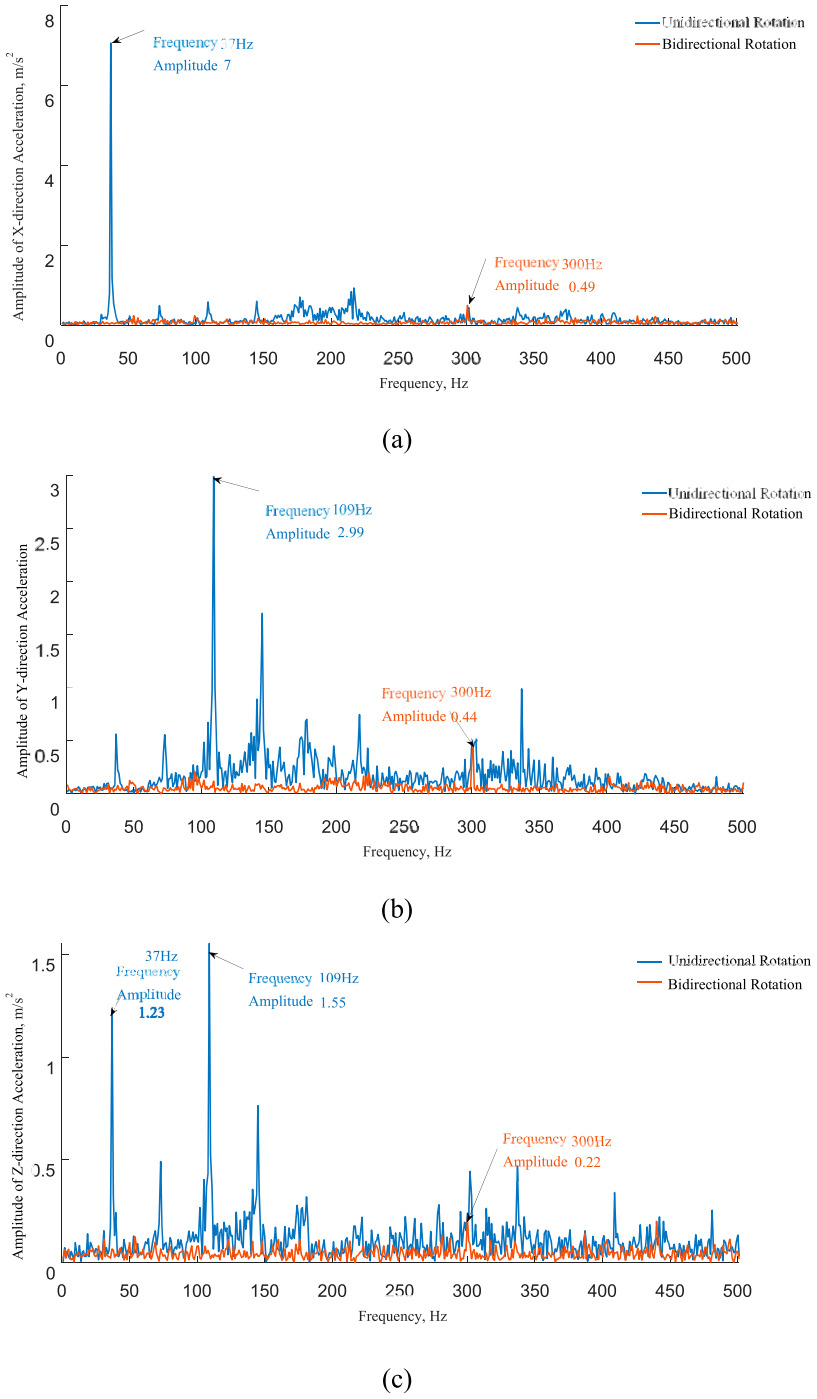

FIGURE 12
Frequency amplitude curve of the single rotation and contra-rotating drilling tools at 60 r/min. (**(a)** X direction; **(b)** Y direction; **(c)** Z direction).

reaction force of this constraint acts at a single point. For a unidirectional drill bit (Figure 13a), this point is denoted as O_1. This point represents the instantaneous center of rotation or the point of application of the resultant constraint force that resists the movement of the rock unit when it undergoes rotational or prying failure during the cutting process. Point O is the point of net force action on the rock unit by the drill bit, and point O_2 is the rotation axis of the drill bit. Therefore, OO_1 is the distance from the net force point of the single tooth of the drill bit on the rock unit to the fulcrum, with $OO_1 = s$, and OO_2 is the distance from the net force point of the cutting teeth on the rock unit to the rotary axis of the bit, with $OO_2 = l$.

To analyze the load on the drill bit teeth, we simplify the failure modes of the rock unit. For a unidirectional rotating drill bit (Figure 13a), the cutting tooth applies a force F_d to the rock. This force can be decomposed into a tangential component

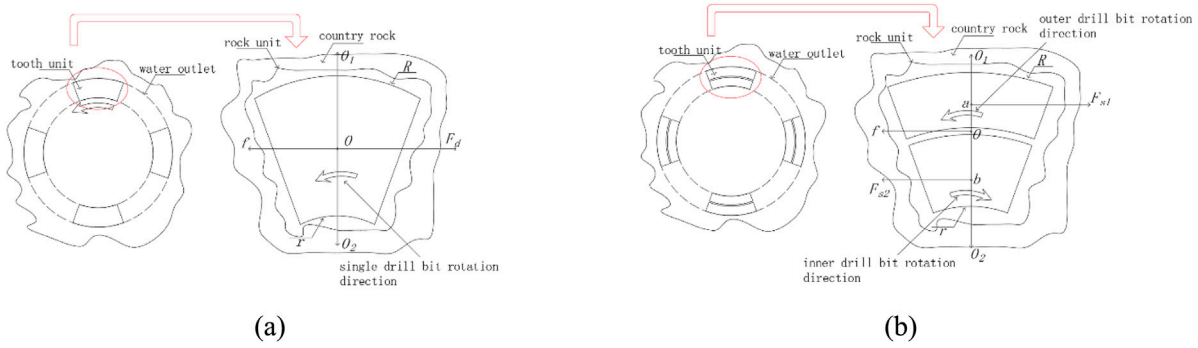

FIGURE 13
Schematic diagram of local stress of rock cutting with single tooth of single and double bit. ((**a**) single drill bit; (**b**) contra-rotating drilling bit).

(primarily causing shear) and a normal component. The normal component creates a moment that causes the rock unit to rotate around its constrained area at the bottom. To quantify this effect, we simplify the constraint reaction force from the underlying rock mass on the rock unit to a concentrated force acting at a single point O_1. Hence the torque received by the drill bit from the rig is M_z. Therefore, the functional relationship between the parameters can be derived as shown in Equation 1:

$$F_d = M_z / l \tag{1}$$

The net moment of a single bit tooth on the rock block is M_d:

$$M_d = F_d s \tag{2}$$

For the contra-rotating drilling tool, point a is the net force point of a single tooth of the outer bit on the rock unit, point b is the net force point of the single tooth of the inner bit on the rock unit, and the distance of ab is e. Point O is in the middle of a and b. The reaction force from the rock unit to the single tooth of the outer drill bit is F_{s1}, which is in the same direction as F_d. The single tooth of the inner bit is subjected to the reaction force from the rock unit, with a magnitude of F_{s2}, and the direction is opposite to F_{s1}. The net reaction force of the rock unit F_d is $F_d = F_{s1} + F_{s2}$ as shown in Equation 3. The rotary torques of the outer and inner drill bits are M_{z1} and M_{z2}, respectively, and the two directions are opposite to one another. Then, we have the following:

$$\begin{cases} F_{s1} = M_{z1} / (l + e/2) \\ F_{s2} = M_{z2} / (l - e/2) \end{cases} \tag{3}$$

The rock unit is subjected to the resultant moment of the single tooth of the two bits M_s:

$$M_s = (F_{s2} - F_{s1}) s \tag{4}$$

It is assumed that the maximum resistance moment produced by the surrounding rock on the calculated rock unit is M_c, where f is the maximum resistance on the rock during the cutting process. Thus, we have the following:

$$M_c = f s \tag{5}$$

During the drilling process, the rock is damaged when the torque or force exceeds the maximum bearing capacity. Equations 2, 4, 5 indicate that, to break rocks, the single rotation drill bit must satisfy $M_d \geq M_c$ $(f \geq F_d)$, and the contra-rotating drill bit needs to satisfy $M_s \geq M_c$ $(f \geq (F_{s2} - F_{s1}))$. As shown by $F_d = F_{s1} + F_{s2}$, F_d is significantly greater than $F_{s2} - F_{s1}$; accordingly, the lower limit of rock cutting in the hole by the contra-rotating drill bit is significantly lower than that of the single rotation drill bit. In terms of the failure mode, the rock between the inner and outer diameters of the single drill bit is dominated by shear stress failure, whereas the rock at the middle annulus of the bit is dominated by compressive stress failure. For dual bits, two distinct failure patterns characteristic of single bits occur within the contact zone between the rock mass and each individual tooth of the dual bits; however, these failures exhibit opposing stress directions. Consequently, rock failure at the outer bit's outer diameter, the outer bit's inner diameter, the inner bit's outer diameter, and the inner bit's inner diameter is dominated primarily by shear stress failure. In contrast, rock failure within the two annular zones of the bits is predominantly characterized by compressive stress failure. The shear strength of most rocks is lower than their compressive strength; therefore, the greater the shear stress zone created by the drill bit on the rock is, the easier it is to break the rock. Based on this principle, a dual-drill-bit system can achieve rock-breaking effects that are similar to those of a single-drill-bit system with less external force, and this reduction in external force is the key mechanism underlying the lower vibrations.

7 Conclusion

In this paper, considering that the contra-rotating drilling method can reduce anti-torque and improve drilling stability, the structure of the contra-rotating drilling tool was designed, and physical tests were conducted to evaluate the amplitude and characteristics of the vibrations of this drilling tool during the drilling process. The main conclusions of this research are as follows:

1. The structural design of the contra-rotating drilling tool was completed, and the gear structure, seal structure, and bearing structure of the contra-rotating drilling tool were designed and fabricated;

2. Based on the results of the drilling vibration test, the vibration of the conventional single rotation drilling tool in the X, Y, and Z directions in the time domain was significantly greater than the corresponding vibration of the contra-rotating drilling tool, and the greater the rotational speed is, the larger the difference in vibration acceleration. In the frequency domain, the vibration amplitude of the contra-rotating drilling tool was much lower than that of the single rotation drilling tool, and with increasing rotation speed, the vibration amplitude significantly decreased;
3. According to the force analysis of the drilling process, under the same stratum conditions, the driving force required for the contra-rotating drill bit to fracture rock is less than that of the single rotation drill bit, which is the main reason that the drilling vibration of the contra-rotating drill bit is much lower than that of the single rotation drill bit.

This study aims to verify the inherent vibration reduction advantages of reverse-rotation drill string structures compared to traditional structures. Therefore, homogeneous artificial rock samples were used to control variables, with mechanical parameters designed to simulate typical soft to medium-hard rock formations. This design allows us to clearly attribute vibration differences to the drill string structure itself, rather than formation variations. However, it must be noted that this study does not cover the effects of different lithologies (such as extremely hard rock, highly plastic mudstone, or highly abrasive sandstone) on the results. Future research will systematically modify the uniaxial compressive strength, internal friction angle, and abrasiveness of the rock samples to establish a more comprehensive drill string-formation adaptability model, further validating the universality and effectiveness of this design under different geological conditions.

Data availability statement

The original contributions presented in the study are included in the article/supplementary material, further inquiries can be directed to the corresponding authors.

Author contributions

LQ: Writing – original draft. LX: Writing – review and editing, Writing – original draft. LH: Writing – review and editing, Writing – original draft. ZZ: Writing – original draft, Writing – review and editing. DH: Writing – original draft, Writing – review and editing. LG: Writing – review and editing, Writing – original draft. ZH: Writing – review and editing, Writing – original draft. FX: Writing – original draft, Writing – review and editing. ZY: Writing – review and editing, Writing – original draft.

Funding

The author(s) declared that financial support was received for this work and/or its publication. This study was financially supported by the project of research and development of a digital engineering survey and drilling equipment and its industrialization (No. 2320004002792) from Zhuhai Industry-University-Research Cooperation Project.

Conflict of interest

Authors LX and DH were employed by Guangdong Eagler Geological Equipment Technology Co., Ltd.

Author LG was employed by Guangdong Ruibo Architectural Design and Research Co., Ltd.

Author FX was employed by Guangdong Zhenzheng Construction Engineering Testing Co., Ltd.

The remaining author(s) declared that this work was conducted in the absence of any commercial or financial relationships that could be construed as a potential conflict of interest.

Generative AI statement

The author(s) declared that generative AI was not used in the creation of this manuscript.

Any alternative text (alt text) provided alongside figures in this article has been generated by Frontiers with the support of artificial intelligence and reasonable efforts have been made to ensure accuracy, including review by the authors wherever possible. If you identify any issues, please contact us.

Publisher's note

References

Abdelbasset, K., Mohamed, G., Shady, S. R., and Sassi, S. (2022). Hybrid fuzzy sliding mode for stick-slip suppression in drill string systems. *J. Mech. Sci. Technol.* 36 (3), 1089–1102. doi:10.1007/s12206-022-0202-y

Bailey, J. R., and Remmert, S. M. (2010). Managing drilling vibrations through BHA design optimization. *SPE Drill. & Complet.* 25 (4), 458–471. doi:10.2118/139426-pa

Cai, Z., Lai, X., Wu, M., Lu, C., and Chen, L. (2022). Equivalent-input disturbance-based robust control of drilling trajectory with weight-on-bit uncertainty in directional drilling. *ISA Trans.* 127, 370–382. doi:10.1016/j.isatra.2021.08.032

Dong, G. J., and Chen, P. (2016). A review of the evaluation, control, and application technologies for drill string vibrations and shocks in oil and gas well. *Shock Vib.* 2016, 7418635. doi:10.1155/2016/7418635

Feng, T. H. (2019). *Modeling and control of drillstring dynamics for vibration suppression*. Austin: The University of Texas at Austin.

Gao, D., and Huang, W. (2024). Basic research progress and prospect in deep and ultra-deep directional drilling. *Nat. Gas. Ind.* 44 (1), 1–12. doi:10.3787/j.issn.1000-0976.2024.01.001

Hegde, C., Millwater, H., Pyrcz, M., Daigle, H., and Gray, K. (2019). Rate of penetration (ROP) optimization in drilling with vibration control. *J. Nat. Gas Sci. Eng.* 67, 71–81. doi:10.1016/j.jngse.2019.04.017

Hu, Z. Q., Zhu, X. H., and Wang, H. (2022). Application of shock absorber based on bit-rock interaction. *China Pet. Mach.* 50 (10), 8–13. doi:10.16082/j.cnki.issn.1001-4578.2022.10.002

Huang, X., Yang, X., and Li, J. H. (2019). Design of adaptive control system based on model reference stick slip vibration. *Bull. Sci. Technology* 35 (4), 129–134. doi:10.13774/j.cnki.kjtb.2019.04.023

Jia, Y. L. (2021). Research on vibration reduction of drill pipe system based on piezoelectric active control technology. *South Agric. Mach.* 52 (22), 114–116.

Lu, C. D., He, Z. Q., Chen, L. F., Li, Q., and Wu, M. (2023). Suppressing coupled axial–torsional vibration of drill-string system considering regenerative cutting induced delay and actuator saturation. *IEEE Trans. Industrial Electron.* 70 (11), 11608–11617. doi:10.1109/tie.2022.3231288

Lv, Y. P. (2020). *Optimization design and vibration characteristics of shock absorber for cylinder type LWD tool*. Lanzhou: Lanzhou University of Technology.

Ma, S., Wu, M., and Chen, L. F. (2023). A robust integrated control design for weight-on-bit fluctuation suppression in drilling process subject to fractured formations. *ISA Trans.* 136, 223–234. doi:10.1016/j.isatra.2022.10.029

Maclean, J. D. J., Vaziri, V., Aphale, S. S., and Wiercigroch, M. (2022). Suppressing stick–slip oscillations in drill-strings by modified integral resonant control. *Int. J. Mech. Sci.* 228, 107425. doi:10.1016/j.ijmecsci.2022.107425

Noabahar Sadeghi, A., Arikan, K. B., and Özbek, M. E. (2022). Modelling and controlling of drill string stick slip vibrations in an oil well drilling rig. *J. Petroleum Sci. Eng.* 216, 110759. doi:10.1016/j.petrol.2022.110759

Ritto, T. G., and Ghandchi-tehrani, M. (2019). Active control of stick slip torsional vibrations in drill-strings. *J. Vib. Control* 25 (1), 194–202. doi:10.1177/1077546318774240

Tashakori, S., Vossoughi, G., Zohoor, H., and van de Wouw, N. (2022). Prediction based control for mitigation of axial–torsional vibrations in a distributed drill-string system. *IEEE Trans. Control Syst. Technology* 30 (1), 277–293. doi:10.1109/tcst.2021.3065669

Wang, H. G., Gao, B., and Zheng, Y. C. (2024). Research progress of machine learning in drill string vibration recognition and prediction. *Nat. Gas. Ind.* 44 (1), 149–158. doi:10.3787/j.issn.1000-0976.2024.01.014

Zhang, X. (2020). *Dynamics, nonlinear instabilities, and control of drill-strings*. College Park: University of Maryland.

Zhou, W. (2021). *Research on torsional vibration characteristics of drill pipe and active vibration absorption control of directional drilling equipment in coal mine*. Xuzhou: China University of Mining and Technology.